JOURNAL OF CATALYSIS 119, 322–341 (1989)

Carbon Deposition and Filament Growth on Fe, Co, and Ni Foils using CH_4–H_2–H_2O–CO–CO_2 Gas Mixtures

A. SACCO, JR.,[1] F. W. A. H. GEURTS, G. A. JABLONSKI, S. LEE, AND R. A. GATELY

Department of Chemical Engineering, Worcester Polytechnic Institute, Worcester, Massachussets 01609

Received February 7, 1989; revised April 7, 1989

Nonequilibrium phase diagrams have been used to systematically investigate carbon deposition and filament growth on Fe, Ni, and Co foils. All three metals were observed to have similar slow rates of carbon deposition in the metal phase field. The carbon formed was primarily amorphous and platelet in type and morphology. In regions where carbides were thermodynamically favored to form, carbon deposition rates were orders of magnitude higher for Fe and Co foils. In the carbide phase field, the rate of fractional weight gain was highest at the highest carbide decomposition temperature and became progressively lower as the carbide decomposition temperature dropped. The order was Fe ≫ Co ≫ Ni. Carbon deposition in the carbide region for Fe and Co produced filaments and amorphous carbon and showed little or no site preference. Carbon deposition on Ni was plane specific and in the carbide region was primarily filamentous in morphology. The primary source of carbon on Ni is CH_4, while on Fe and Co it appears to be CO. The role of carbides on these foils is hypothesized to be to increase surface area through surface break-up, and to help set up the mass flux gradient for filament growth.

INTRODUCTION

When carbon-bearing gases contact transition metals at high temperature, filamentous carbon often forms. For many years, work has been performed to try to prevent its formation because it destroys metal integrity and has destroyed many industrial catalysts. Recently, however, work has been under way to determine how to produce filamentous carbon of uniform dimension and in high yield for use in high strength, light weight carbon/carbon composites. Although intensive efforts have been made to understand the initiation and growth mechanisms, these processes are still not clearly understood.

Carbon filaments are uniform in width (between 500–1000 Å) (*1*) and are generally cylindrical in shape, although flat ribbons and twisted filaments (*2*) have been reported. The cyclindrical filaments appear to have a hollow central core. Metallic crystals are often found at the end of these filaments and in some cases metallic fragments are found throughout their length. These metal crystallites are believed to be catalytically active for carbon deposition and are called "growth" crystals. The filament shaft has been reported by Oberlin *et al.* (*3*) to be "tree-like"; consisting of an inner ring of well-ordered carbon adjacent to the hollow core and an outer carbon layer which is less ordered but more dense. The filaments can have lengths over 5 mm (*4*) and BET areas as high as 100 m^2/g (*5*).

The growth mechanism and to a lesser extent the initiation mechanism for filaments have been speculated on by many investigators: Ruston *et al.* (*6*), Baker *et al.* (*7*), Boehm (*2*), Oberlin *et al.* (*3*), Rostrup-Nielsen and Trimm (*8*), Tibbetts *et al.* (*9*), Kock *et al.* (*10*), Sacco *et al.* (*11*), and Alstrup (*12*). However, no complete mechanism has been proposed which can explain the various and often conflicting data. One reason for these discrepancies is that the actual solid (surface ?) composition was not controlled during reaction. Consequently, it is unclear which phase or phases are cata-

[1] To whom correspondence should be addressed.

0021-9517/89 $3.00

TABLE 1

Examples of Actual Gas Compositions Used in Reactions over Fe, Co, and Ni Foils in the Metal and Carbide Regions

Metal	Mole percent					O/H	%C	$\hat{a}_c$
	H_2	CO	CH_4	CO_2	H_2O			
Metal Region								
Fe	49.72	15.64	13.14	8.77	12.72	0.259	14.39	1.58
Co	48.64	17.67	15.52	8.21	9.96	0.246	15.64	2.11
Ni	49.09	15.60	13.36	9.31	12.64	0.265	14.61	1.56
Carbide Region								
Fe	29.65	32.47	30.33	5.53	2.03	0.247	22.89	11.06
Co	29.80	31.80	29.94	5.32	3.15	0.246	22.48	9.55
Ni	28.89	32.18	29.95	5.99	2.98	0.257	22.81	9.54

lytic for filament growth. Also, it is well known that the structure of a metal (alloy), and indeed its composition in the case of carbon-bearing alloys, is a strong function of its time–temperature history. Thus, depending on the original reactor temperature and the original metal composition, the cool-down history in the reactor could have radical effects on the observed structure and resulting proposed mechanism.

Work in our laboratory (*11, 13, 14*) has been directed at controlling the solid "surface" composition using phase diagrams.[2] This approach has proven successful in studying filament growth in the C–H–O–Fe system at high temperature (i.e., 800–900 K, Sacco *et al., 11*). High temperature is necessary to minimize the difference between surface and bulk composition. These investigations have been continued on Ni and Co foils.

METHODOLOGY

The methodology used to study carbon deposition and filament growth in this work was identical to that described elsewhere (*11, 13*). Only a brief description will be presented here to enhance the understanding of the data presented. When used properly, this approach can prove useful in understanding complex multicomponent solid–fluid reaction systems.

Phase diagrams were used to systematically control *in situ* the gas-phase chemical potentials (activities), and thus control the solid surface thermodynamically favored during carbon deposition. The solid metal phase can be more easily controlled using multicomponent gas mixtures. The five gases chosen represent reaction gases frequently encountered in industrial applications. An example of the actual gas compositions used is shown in Table 1. Figure 1 represents a typical phase diagram for the $Ni/Ni_xC/NiO/C_\beta$/gas (CO_2, CO, CH_4, H_2, H_2O) equilibrium at 900 K and 1 bar pressure. The data of Manning *et al.* (*15*) was used to generate the position of the Ni_xC phase boundary (dashed line). All the remaining phase boundaries were generated from free energy data obtained from the JANAF tables (*16*). The solid curve concave upwards represents the gas/C_β equilibrium curve.[3] The straight line between

[2] The terminology "phase diagram" as opposed to equilibrium phase diagram is used since metastable phases (e.g., carbides) are included.

[3] It is recognized that the form of carbon deposited during reactions (filaments, platelets, etc.) may not be graphitic (*17*). However, using the data of Rostrup-Nielsen (*18*), DeBokx *et al.* (*19*), and Manning *et al.* (*15*) at 900 K, it is found that the effect on the equilibrium is not great, and, for all intents and purposes, the gas compositions are identical to those determined using graphite.

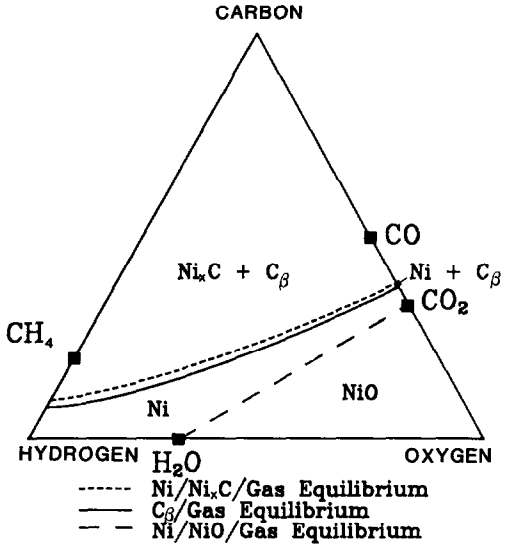

FIG. 1. Ni–C–H–O phase diagram (900 K and 1 bar pressure).

the position of H_2O and CO_2 on the diagram represents the Ni/NiO/gas equilibrium. These equilibrium phase boundaries divide the triangular surface into regions which thermodynamically favor the solid phase(s) shown. Any gas mixture composed of CO, CO_2, H_2O, CH_4, and H_2 can be plotted on this triangular surface. Depending on the gas mixture's carbon activity,[4] hydrogen activity, and/or oxygen activity (i.e., position on the triangular surface), carbide(s), reduced metal, oxide(s), or a combination of these will be thermodynamically favored. Thus, if one of these phases is already present or if the kinetics of formation of the phase is fast relative to the reaction(s) being investigated, one can study which phases are catalytic for which reactions. Therefore, within broad limits, one can fix the gas phase activity while simultaneously varying the relative amounts of CO, CH_4, CO_2, H_2O, and H_2 to observe how specific solid phases catalyze specific carbon depositing reactions. In using these diagrams, one must be careful not to unintentionally change phase fields. This necessitates running reactions differentially, with careful heating and cooling procedures, and precise gas feed rates and compositions.

[4] Example of activity calculation

$$2CO \rightleftharpoons CO_2 + C_\beta.$$

To obtain a numerical value for the equilibrium constant for the desired reaction, at the temperature and pressure of interst: $K_{eq} = \hat{a}_{CO_2} \cdot a_{(C_\beta)}/(\hat{a}_{CO})^2$.

$\hat{a}_{C\ Gas\ Phase} = K_{eq}/Q$, where $Q = P_{CO_2}/(P_{CO})^2$ (actual conditions).

TABLE 2

Typical Impurity Concentrations for As-Received Ni and Co Foil (Johnson Matthey, Inc.)

	Impurity	PPM by weight
Co foil		
	Ca	10
	Si	3
	Al	1
	Fe	1
Ni foil		
	Si	2
	Al, Ca, Cu, Fe, Mg, Ag	<1

EXPERIMENTAL

All experiments were performed using pure Ni(99.9975%) or pure Co(99.9965%). Table 2 lists the impurity concentrations in both metals. Foils were received in large 0.1-mm-thick sheets (Johnson Matthey, Inc.). These were cut to 6 × 6-mm squares using a Bridgeport milling machine. In one corner of each square foil a 1-mm hole was drilled to allow each sample to be suspended in the furnace. To remove extraneous hydrocarbons from the foils, all samples were ultrasonically cleaned with acetone prior to introduction into the reactor. Generally, to begin an experiment, the apparatus was flushed with He (10 cm^3/s, STP) for 30 min, then heated to a temperature in pure H_2 (15 cm^3/s,STP) for 3 h prior to the introduction of reaction gases. Precise gas concentrations were fed to the reactor at a volumetric flow rate of 20 cm^3/s, (STP). Typically, experiments were run for between 3 and 8 h, weight gain being con-

tinuously monitored. Depending on experimental objectives, several different cool-down procedures were available for use. The foils could be quench cooled with liquid N_2 or by heat exchange with cryogenically cooled H_2. These procedures were employed to "freeze-in" solid phase compositions. When solid phase identification was unimportant, a slow cool-down procedure in an inert environment was used.

(A) *Apparatus*

Two reactor units were utilized during this investigation. The first is similar to that previously described by Sacco and Caulmare (*13*). The reactor assembly was supported on an isolation platform. This allowed continuous monitoring of the foil's weight change ($\pm 10^{-6}$ g) using a Cahn 2000 electrobalance. The reactor was operated isothermally using a West SCR stepless proportional controller. Reactor temperature was controlled to $\pm 1°$ K up to 900 K, with the reactor pressure maintained at approximately 1 bar. Water was introduced into the gas stream by using water baths and working off the 100% saturation curve at a given temperature. Gas compositions were monitored periodically using an on-line Sigma-1 gas chromatograph.

In addition to the reactor, which continuously monitors carbon deposition, a second reactor was constructed to rapidly quench foils under reaction conditions. This reactor utilized the same feed gas delivery system as the previous reactor. The reactor itself was "U" shaped. It was located in a furnace and temperature was controlled to $\pm 1°$ K. Samples were rapidly moved from the reaction zone to the quench section and cooled in the cryogenic heat exchanger to ambient temperature in under 10 s. For more rapid cooling, the sample could be drawn directly from the reaction environment into a liquid N_2 bath.

(B) *Solid Phase Identification*

Foils were examined before and after reaction using optical and electron microscopy. Transmission electron microscopy (TEM) was performed using a JEOL-100C STEM, with an operational resolution of 3–10 Å. Samples were prepared from extracted replicas or the foils were observed on edge. Scanning electron microscopy (SEM) was performed using a JEOL 840 SEM. X-ray diffraction (XRD) patterns were obtained directly from the reacted Ni and Co foils using Ni-filtered Cu$K\alpha$ radiation for Ni, and Fe-filtered Co$K\alpha$ radiation for the Co samples. These data were obtained using a General Electric X-ray diffractometer.

RESULTS AND DISCUSSION

Generally, all experiments were performed a minimum of three times at three or four different O/H ratios. Solid symbols represent weight gain attributed to carbon deposition, while open symbols represent weight loss (i.e., carbon gasification). Also, circular symbols are used for runs at an O/H ratio of 0.25, squares for an O/H ratio of 0.67, crosses for an O/H ratio of 1.22, and triangles for an O/H ratio of 2.33. When comparisons between these three metals are made, solid symbols are used for Fe, partially filled symbols for Co, and open symbols for Ni.

An initial experiment using only an inert quartz substrate indicated that at 900 K and 1 bar pressure, no gas-phase carbon deposition was observed. This was substantiated when, after many different gas mixtures were run over metal foils, no carbon deposit was observed on the reactor walls. Therefore, it was concluded that carbon deposited on the foils was the result of catalytic decomposition only.

(A) *Cobalt*

Figure 2 is an expanded portion of the $Co/Co_3C/CoO/C_\beta$/gas-phase diagram at 900 K and 1 bar pressure. As illustrated, weight gain was observed in both the reduced metal region and the carbide phase field. Carbon gasification also was observed in the reduced metal region. Solid-phase

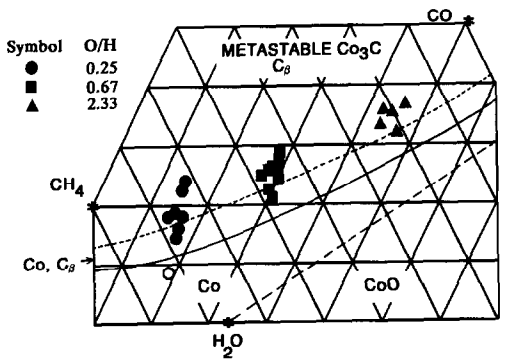

FIG. 2. Cobalt/cobalt carbide/cobalt oxide/carbon gas equilibria at 900 K and 1 bar pressure (solid symbols indicate weight gain; open symbols indicate weight loss).

identification was performed on quench-cooled (1–7 s) samples using XRD. Figure 3 shows a series of XRD patterns of Co foils exposed to pure H_2, a gas mixture which supports both carbon deposition and a reduced metal surface (O/H = 0.25, $\hat{a}_c = 3.0$), and a gas mixture which supports both carbon deposition and a thermodynamic driving force for carbide formation (O/H = 0.25, $\hat{a}_c = 10.0$). All three experiments were performed at 900 K and 1 bar pressure. Several features are of interest. First, none of the additional peaks in Fig. 3c are from carbides. This is not unexpected since the decomposition temperature reported by Nagakura (*20*) and Hofer *et al.* (*21*) for Co_3C is ≈750 K. Also, even though the chemical potential driving force would predict Co_3C formation, quench cooling would be likely to dissociate the metastable phase. Second, a graphite peak is present in the XRD pattern of the "carbided" metal foils. Finally, hydrogen treatment and the associated cooling sequence results in little change from the room temperature α (HCP) structure of Co. However, under carbon-depositing conditions, the favored (900 K) HCP → FCC transition occurs (d = 1.7723, 60.70° 2θ). This suggests that the "carbon" deposited, or the environment from which it comes, either encourages the formation of the high-temperature phase or stabilizes it. This transformation occurs rapidly—under 10 min at reaction conditions. This could be significant if preferential order of structure (planes) was shown to be of importance for carbon deposition on Co.

Figures 4a and 4b illustrate the type of carbon deposition behavior observed. Figure 4a is a plot of weight gain, corrected for the initial surface area, versus time for metal foils in the reduced metal-phase region. As shown, there is no induction period and there is not a substantial difference (reproducibility ±25 μg) in weight gain as one moves across the phase diagram. In other words, as one moves from regions of relatively high CH_4 and H_2 contents (and conversely low CO contents) at an O/H equal to 0.25 to regions of relatively low CH_4 and H_2 contents (high CO contents) at O/H equal to 2.45, no significant change in deposition rate is observed. A simple power law kinetic argument would suggest this behavior is likely to be the result of a reaction of the form

$$CO + H_2 \rightarrow H_2O + C_\beta. \qquad (1)$$

This hypothesis is further substantiated by the fact that the weight gain curves, if they differ at all, increase in proportion to the $P_{CO}P_{H_2}$ product.

In the carbide region, the behavior was quite different. Figure 4b is a plot of weight gain in the carbide region versus time for Co foils at various O/H ratios. The rate of carbon deposition was substantially higher, by over one order of magnitude, than that observed in the reduced metal region. Also, after approximately 275 min, the amount and rate of weight gain was highest at the lower O/H ratio. Figure 5, which is a plot of the rate of fractional weight gain (RFWG) versus time, best illustrates these points. These data indicate that the slope of the initial portions of the RFWG curves seems to correlate to the $P_{CO}P_{H_2}$ product. However, the steady-state portion of the RFWG curves presented a different order, correlating instead to the gas-phase O/H ratio. After the initiation period the maxi-

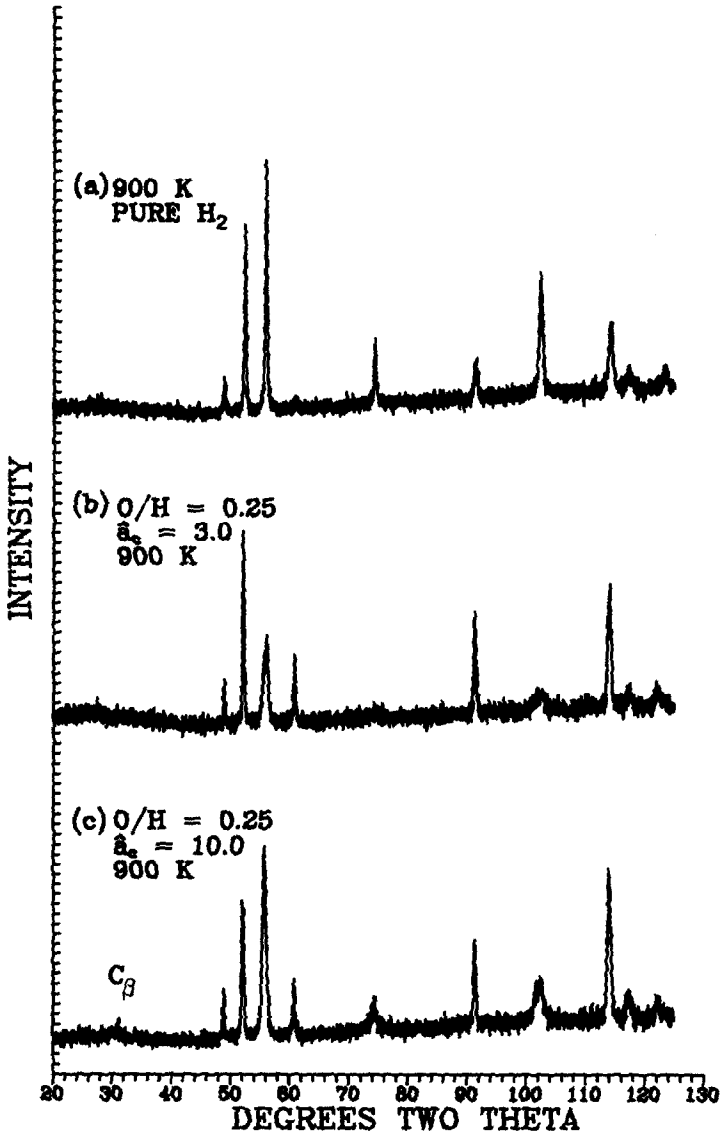

FIG. 3. XRD patterns of (a) reduced Co, (b) Co reacted in the metal region, and (c) Co reacted in the carbide region (Co$K\alpha$ radiation).

mum rate of fractional weight gain (steady-state portion), for an essentially fixed carbon gas-phase activity, was observed to increase with decreasing O/H ratio. More to the point, reactions which use CH_4 as their carbon source may be hypothesized to deposit carbon more rapidly than do reactions which use CO as their carbon source. Another possible hypothesis is that the relatively high hydrogen contents at low O/H ratios results in a "cleaner" surface for the active species to adsorb and react. These data do, however, cast some doubt on the assumption of Audier *et al.* (*22–24*) that carbon deposition and the associated filament growth rate are linear functions of the gas-phase carbon activity. In these experiments, the gas-phase composition is changed at a relatively fixed gas-phase carbon activity and the RFWG is observed to

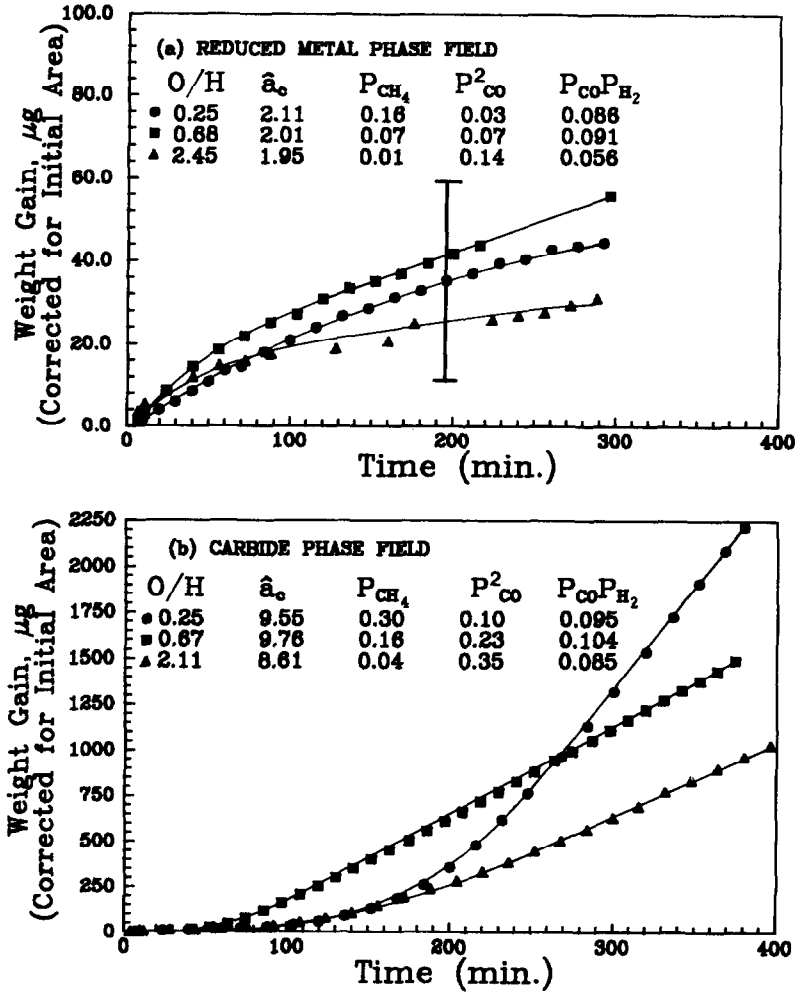

FIG. 4. Normalized weight gain vs time over Co foils at different O/H ratios and 900 K and 1 bar pressure. (a) Reduced Co phase field and (b) Co_3C phase field.

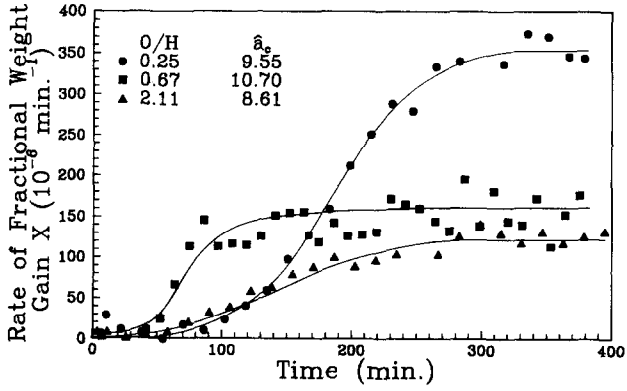

FIG. 5. Rate of fractional weight gain vs time over Co in the carbide region at various O/H ratios (900 K and 1 bar pressure).

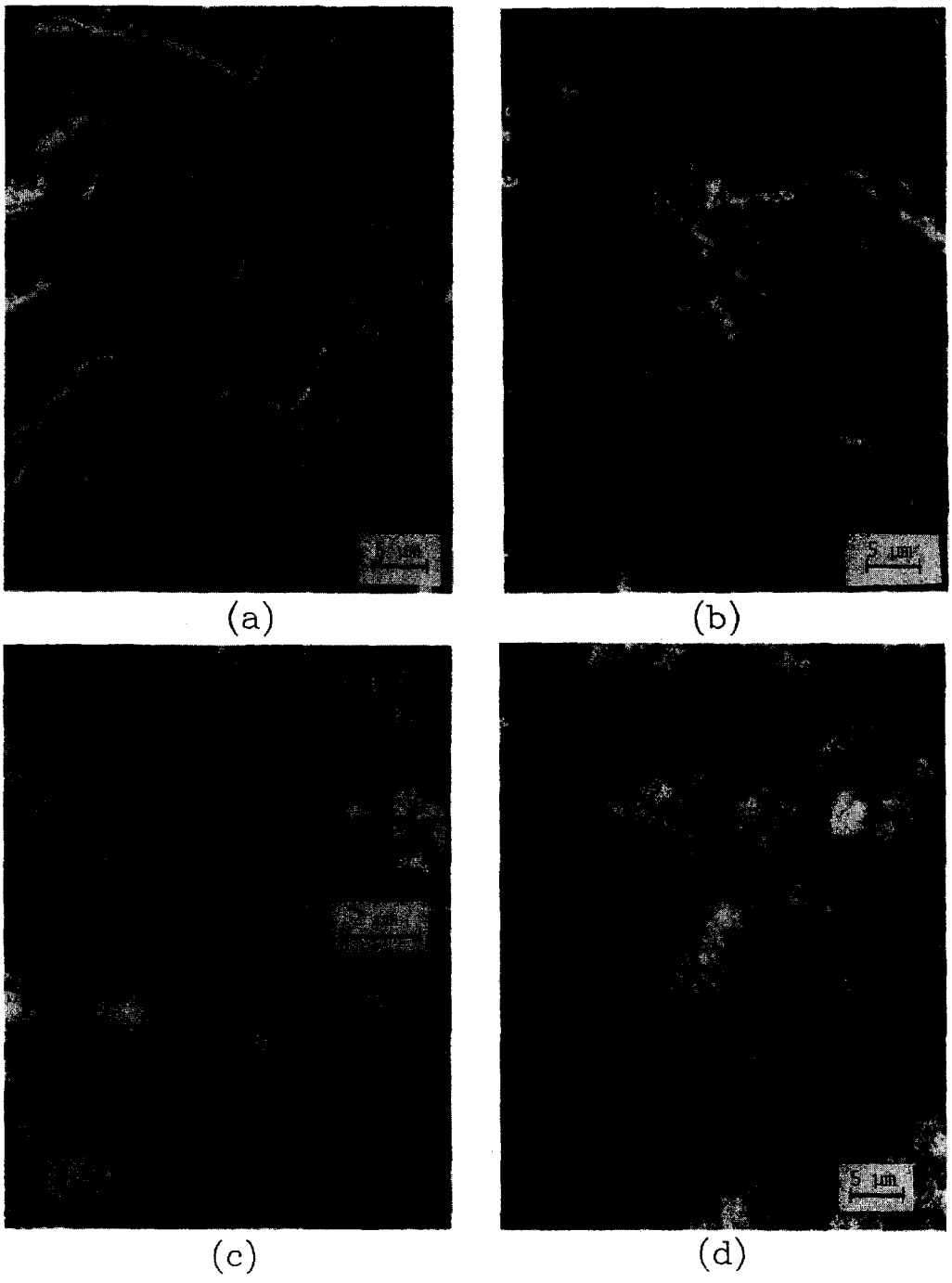

FIG. 6. Quenched Co foils at various stages of reaction. O/H = 0.25, $\hat{a}_c$ = 10, 900 K, and 1 bar pressure.

change (Fig. 5). However, as is always the case with carbon deposition, many different forms of carbon appear to form simultaneously with filaments (Fig. 6). Therefore, the assumption by Audier *et al.* (*22–24*) concerning the filament growth mechanism may still be a viable one.

Figure 6 presents a series of electron mi-

crographs of typical Co foils under reaction conditions as a function of time. These experiments were carried out at 900 K, 1 bar pressure, O/H = 0.25, and a gas-phase carbon activity of 10. At time 0 (Fig. 6a), the surface appears to have a randomly oriented "ripple-like" texture with several prominent grain boundaries. After the foil is exposed to the reacting environment for 5 min (6b), a thin carbon overlayer has formed. Through this overlayer, "cauliflower-like" eruptions begin to appear. At 160 min, the RFWG curves (Fig. 5) show a rapid increase; simultaneously, micrograph 6c shows a large population of "cauliflower-like" eruptions. The enlargement of these surface growths depicted in Fig. 6c suggests they consist of amorphous carbon and Co fragments. Micrograph 6d, taken after 256 min exposure, depicts a surface completely covered with these cauliflower bundles. These bundles appear to be composed of amorphous carbon and poorly formed filaments. This initiation and growth behavior is very similar to that observed on Fe foils (*11*). Similar morphologies were observed by Jackson *et al.* (*25*) when H_2–propylene mixtures were pyrolyzed over Ni and Fe–Ni–Cr alloys at temperatures between 873 and 1273 K.

(B) Nickel

Figure 7 is an expanded version of the Ni/Ni_xC/NiO/C_β/gas-phase diagram at 900 K and 1 bar pressure. As was observed with Co foils, weight gain occurred in both the reduced metal and the carbide phase fields. Also, as was shown with Co, gasification of previously deposited carbon occurred in the reduced metal phase region.

The XRD patterns for typical Ni foils under various reaction conditions are illustrated in Fig. 8. The reaction conditions represented are: (a) reduced in H_2 at 900 K for 3 h (including heat-up time), (b) reacted for 3 h at O/H = 0.25 at a gas-phase carbon activity of 1.2 (reduced region), and (c) reacted for 3 h at 900 K at an O/H = 0.67 in the carbide phase field ($\hat{a}_c$ = 10). These data are not dissimilar to those observed for Co. On quenching, no carbides were observed on the foils in the carbide-phase field, but some graphite is present. Once again, the absence of diffraction lines for Ni_3C is understandable since Ni_3C is reported unstable above 573 K (*26*). Unlike Co, the shift in relative intensity of the diffraction lines of various Ni foils after exposure to different reaction environments suggests preferential plane orientation may be important on Ni.

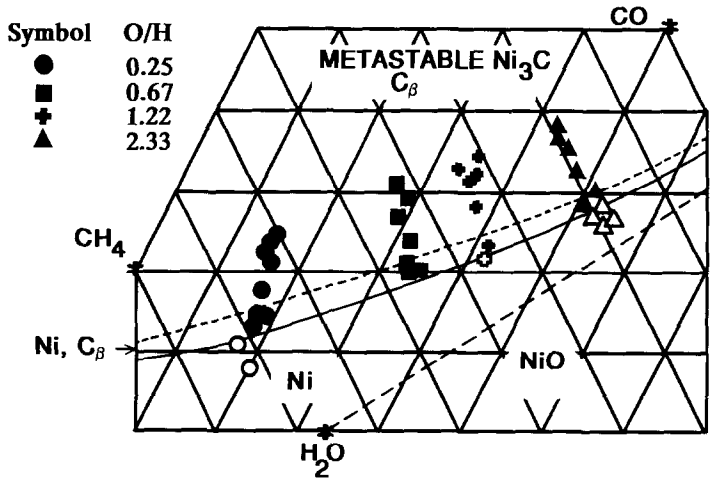

FIG. 7. Nickel/nickel carbide/nickel oxide/carbon gas equilibria at 900 K and 1 bar pressure (solid symbols indicate weight gain; open symbols indicate weight loss).

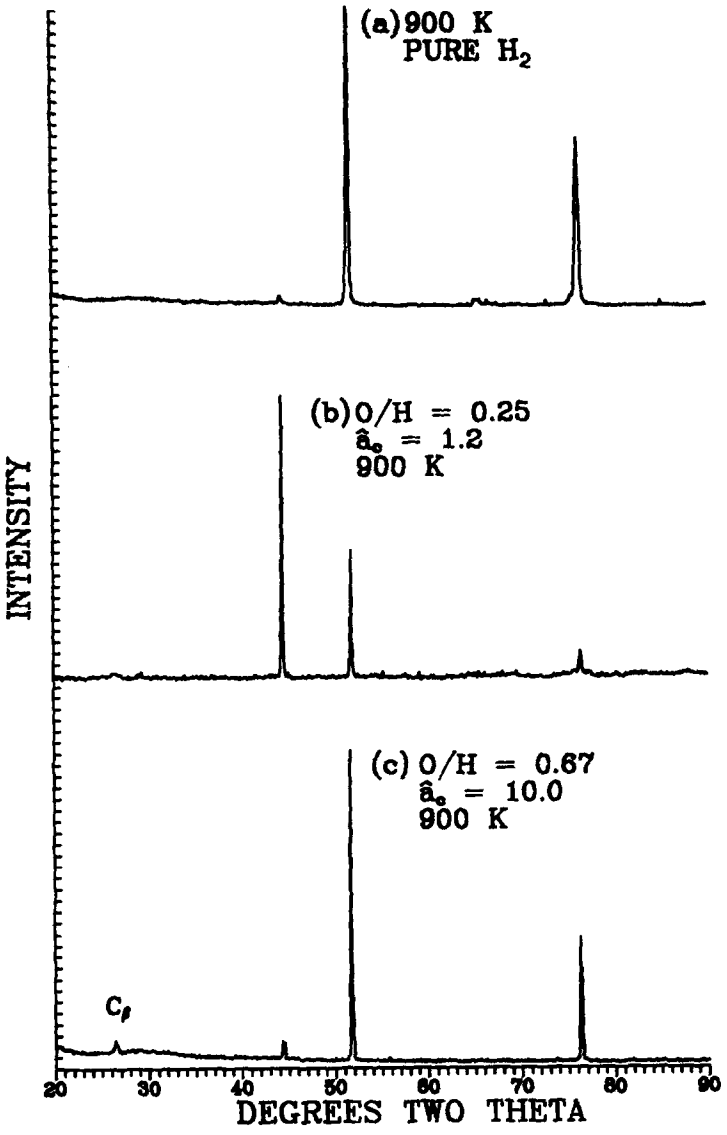

FIG. 8. XRD patterns of (a) reduced Ni, (b) Ni reacted in the metal region, and (c) Ni reacted in the carbide region (Cu$K\alpha$ radiation).

This observation may be magnified due to some planes being selectively covered by carbon. This phenomenon has been reported in the work of Baird *et al.* (*27*), Leidheiser and Gwathmey (*28*), Kehrer and Leidheiser (*29*), and Renshaw *et al.* (*30*). Figure 9 shows several low-magnification electron micrographs that illustrate preferred carbon deposition. This kind of behavior, although observed to a small extent on Co and Fe, was prevalent during all Ni foil experiments.

Figure 10a is a plot of weight gain versus time for various O/H ratios for Ni foils in the reduced metal-phase field at 900 K. As illustrated, within the reproducibility (±25 μg) associated with the weight gain curves, all of the curves are the same. This would suggest that despite very different gas compositions, the controlling mechanism is

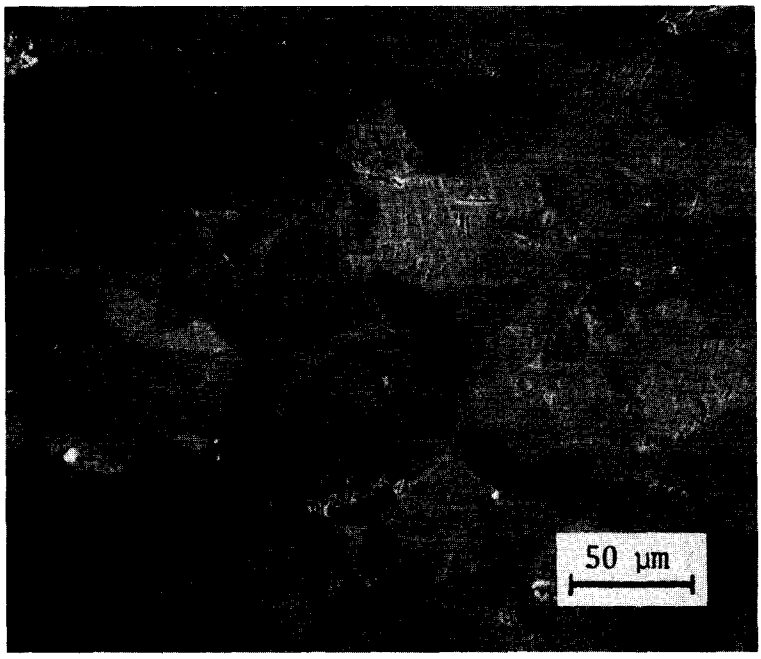

(a)

(b)

FIG. 9. Quenched Ni foils reacted in the carbide region exhibiting preferential carbon deposition (O/H = 0.25, $\hat{a}_c$ = 10, 900 K, and 1 bar pressure).

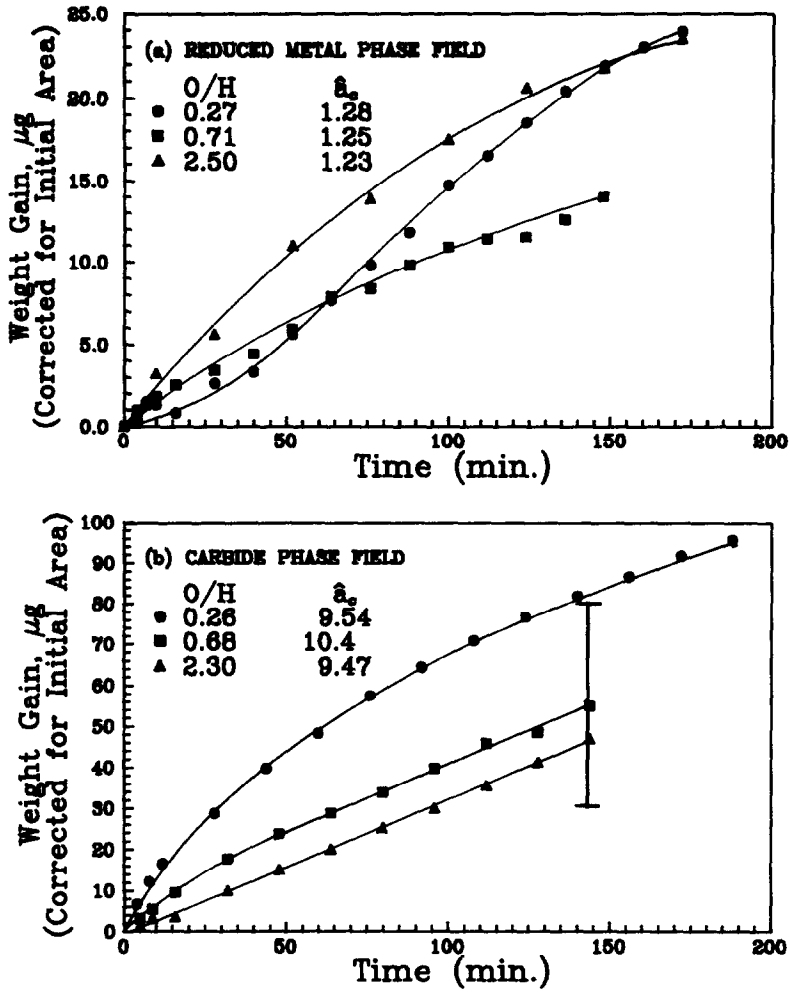

FIG. 10. Normalized weight gain vs time over Ni foils at different O/H ratios at 900 K and 1 bar pressure. (a) Reduced Ni phase field and (b) Ni_xC phase field.

likely to be the same. This could either be a reaction of the type presented by Reaction 1, or the controlling mechanism could be the diffusion of carbon through the base metal, resulting in filament growth.

Figure 11 illustrates the typical carbon formation morphology observed in the reduced metal region. A thin carbon overlayer is observed within which are imbedded spherical Ni fragments and carbon filaments. The filaments are poorly formed and have metal crystals along their entire length. If diffusion was the rate-controlling step for carbon deposition in this phase region, more filaments would be expected; the morphology of the carbon formed (amorphous layered carbon) would suggest kinetic control is probable in the reduced metal region.

In the region where carbides are thermodynamically favored to form, the behavior is similar to that observed in the Co carbide-phase field. That is, the highest weight gain curve seems to be associated with the lowest O/H ratio. This statement is made with caution due to the substantial error bars shown in Fig. 10b. Unlike Co, there is no apparent initiation step, and therefore

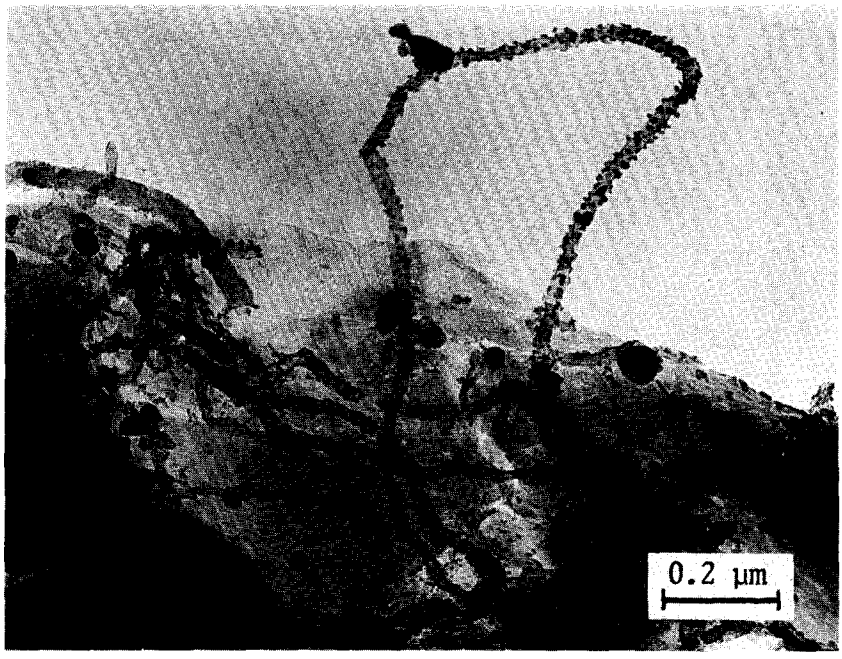

(a)

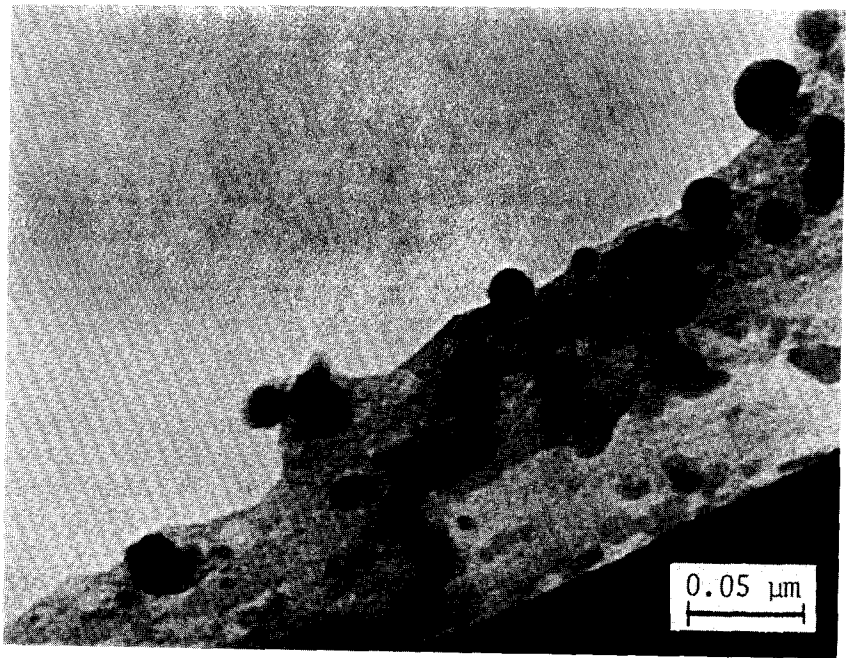

(b)

FIG. 11. Filaments formed over Ni in the reduced metal phase field (O/H = 0.25, $\hat{a}_c$ = 1.2, 900 K, and 1 bar pressure).

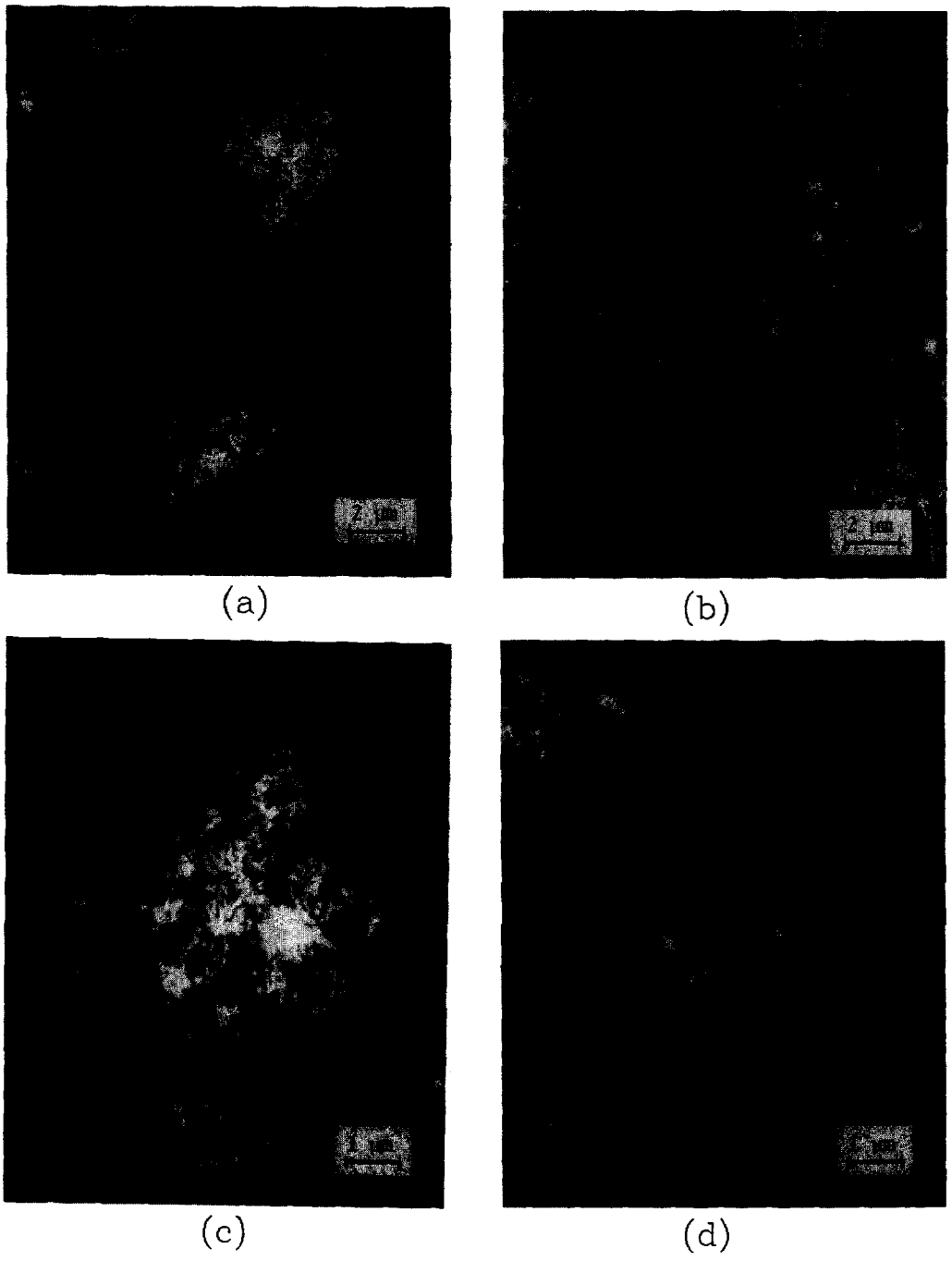

FIG. 12. Quenched Ni foils reacted in the carbide phase field (O/H = 0.25, $\hat{a}_c$ = 10, 900 K, and 1 bar pressure).

the initial weight gain is independent of the $P_{CO}P_{H_2}$ product for Ni.

Figure 12 shows representative Ni foils after a 3-h exposure to reaction gas in the carbide-phase field (O/H = 0.25, $\hat{a}_c$ = 10). As illustrated, there are specific locations on the foils from which bunches of well-formed filaments grow. Very little flake or

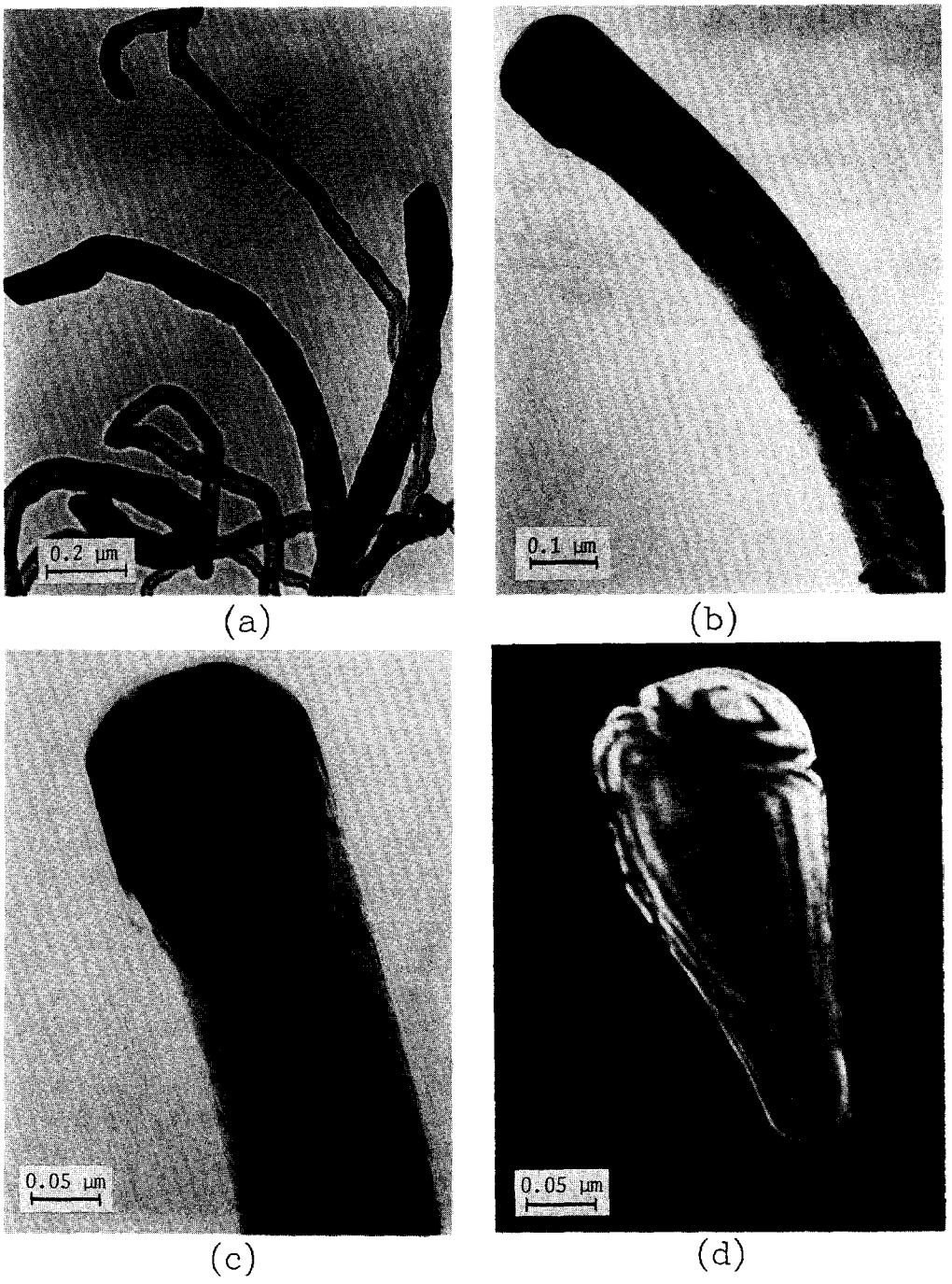

FIG. 13. Filaments formed over Ni in the nickel carbide phase field (O/H = 0.25, $\hat{a}_c$ = 10, 900 K, and 1 bar pressure).

amorphous carbon was observed. This morphology is unlike that observed on Co or Fe, both of which contain substantial flake and amorphous carbon in addition to filaments. Figure 13 shows several high-resolution micrographs of typical filaments

grown over Ni. They are approximately 100 nm in diameter, have a hollow central core, and the crystal tips appear to have a specific orientation. Although unable to identify the crystallographic orientation of these tips, their appearance is similar to those reported by Audier *et al.* (*31*). Also, the light and dark field images of a typical filament tip show what seems to be "cleavage" of the crystal. This "cleavage" may be the birth of another filament. A high-magnification micrograph of the filament shaft shown in Fig. 13b suggests that the growth of these filaments is erratic. It is hypothesized that carbon builds up at the back end of the filament tip pushing the crystal forward until the force is relieved. Then motion stops until enough force is built up to push the crystal forward again. This is the first report of this type of "stepping" growth mechanism that the authors are aware of.

(C) *Cobalt Versus Nickel Versus Iron*

It is illustrative to compare Co, Ni, and Fe carbon deposition behavior in regions where reduced metal or carbides are thermodynamically predicted to form. Figure 14a is a typical plot of weight gain versus

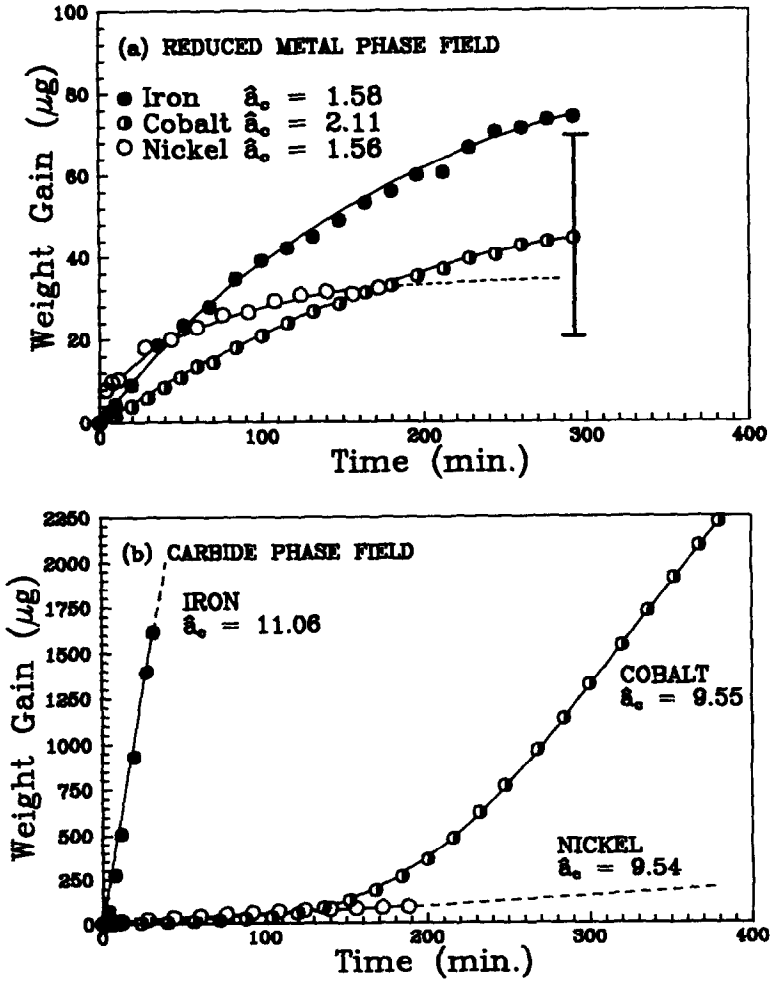

FIG. 14. Weight gain vs time for Fe, Ni, and Co foils at O/H = 0.25, 900 K, and 1 bar pressure. (a) Reduced metal phase field and (b) carbide phase field.

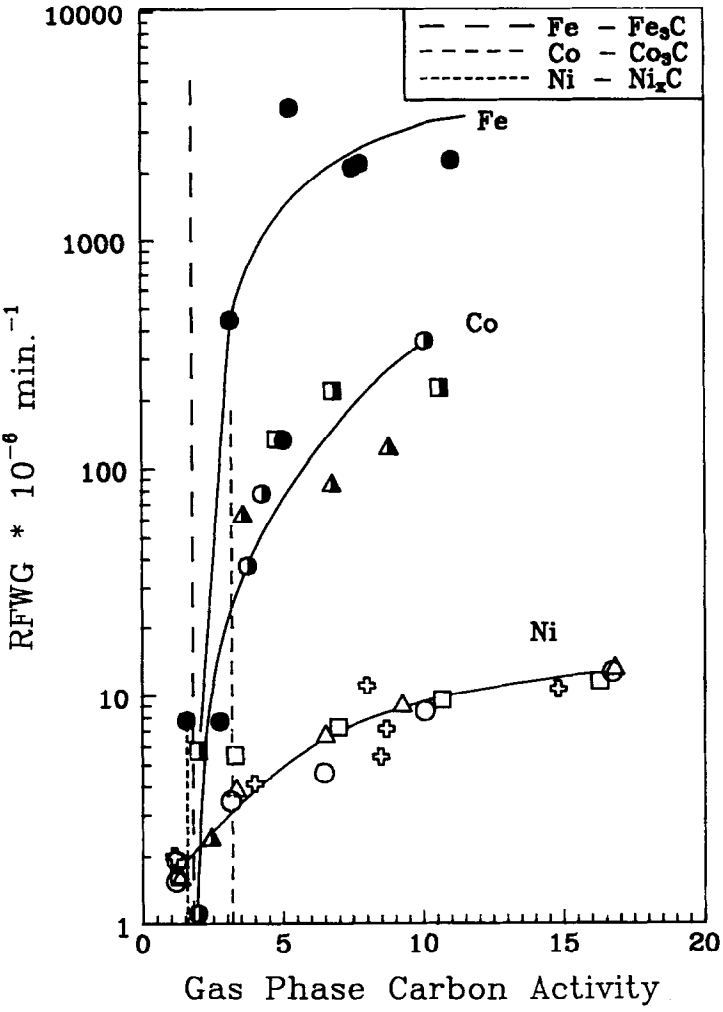

FIG. 15. Rate of fractional weight gain vs carbon gas phase activity for Fe, Ni, and Co foils at various O/H ratios (900 K and 1 bar pressure).

time curves at 900 K and 1 bar total pressure for an O/H ratio of 0.25. The gas-phase carbon activity is such that all three metals are in their reduced metal regions. Considering the errors involved with these data (±25 μg), all three plots are essentially the same, indicating that the three metals are similar catalytically. Figure 14b shows that in the carbide regions the story is quite different. In Fig. 14b are plotted values for weight gain versus time for foils at 900 K, 1 bar, O/H ratio of 0.25, and an activity which places each foil within its carbide-phase field. Although it is difficult to see for Fe, there is an initiation period for both Fe and Co but not for Ni. When plotted as RFWG versus gas phase carbon activity (Fig. 15) several interesting features emerge. First as one crosses from the thermodynamically favored metal regions to the thermodynamically favored carbide regions (vertical dashed lines), the rate of fractional weight gain increases exponentially for Co and Fe, but is only linear for Ni. The near-linear dependency observed for Ni must be tempered since the RFWG for Ni foils is somewhat dependent on the O/H ratio. Figure 15 illustrates that in the

regions where carbides are favored to form, Fe is the most catalytically active for carbon deposition, followed by Co, and finally Ni. It must be remembered, however, that as shown in this work and reported by Sacco *et al.* (*11*) the carbon deposits on the three metals are different. In the cases of Fe and Co foils exposed to reaction gas in the carbide phase field, initially a blanket of carbon covers the surface more or less evenly. It should be noted that in the cases of both Fe and Co, micrographs show that some planes may be more active for carbon deposition than others. These preferential areas are only observed at very early times. In general, all crystallographic orientations in the carbide phase field appear on a macroscopic scale to be good catalysts for carbon deposition. Some time after complete surface coverage, the surface begins to be broken-up by cauliflower-like eruptions. These projections consist of filamentous and amorphous carbon.

For Ni, a thin amorphous layer is observed to form only on specific areas. In the reduced metal region metal fragments and a few poorly formed filaments were favored. In the carbide-phase field, one observes "islands" of well-formed filaments, many of which show specific crystal orientation of the metal filament tip. Although the number of islands increases with time on stream, at no time is the total nickel foil surface covered with filaments.

(*D*) *Mechanism*

In the reduced metal form, Co and probably Fe are modestly catalytic for carbon deposition. Reaction 1 is hypothesized to deposit the observed amorphous overlayer. As one moves from regions that favor the reduced metal to regions where carbides are favored to form, exponential increases in the rates of carbon deposition were observed. This increase in RFWG was shown to initially correlate nicely for both Co and Fe (Sacco *et al.*, *11*) to the $P_{CO}P_{H_2}$ product. As the time of foil exposure in the carbide-phase field increases, carbides are formed and stabilized under compressive stress. The Poynting correction factor predicts a decrease in free energy (improved stability) with an increase in pressure (compressive stress) for an overall decrease in the volume of reaction ($\Delta V°$). A negative volume change occurs when a carbide forms from carbon and the parent metal.[5] However, because the molar volumes of these carbides are larger than those of the parent metals, after a short time the pressure at the grain boundaries and dislocations will exceed the tensile strengths of the parent metals. This is observed on Fe and Co foils as cauliflower-like eruptions; that is, the underlying surface breaks up, erupting through the carbon overlayer. Also, the release of compressive stress will result in carbide dissociation and concomitant graphite precipitation (Fig. 3c). Carbides may be involved catalytically with carbon deposition and filament growth, but it is more likely their role is to increase surface area through surface break-up and to serve to set-up the mass flux for filament growth as described in the works of Sacco *et al.* (*11*), Alstrup (*12*), and Bianchini and Lund (*32*).

Nickel foils appear to behave differently than Co and Fe foils. The weight gain plots show an approximate linear dependence on gas-phase carbon activity. This dependence holds in both the reduced metal-phase field and the carbide-phase field. Unlike Co or Fe, carbon deposition on Ni is relatively slow and appears to occur preferentially on specific grains. The carbon formed is also primarily filamentous. It is unclear why the Ni surface does not break up. Perhaps this is due to the fact that at 900 K, Ni_3C is the least stable of the three transition metal carbides, and therefore compressive stress cannot build up to support its stability. In any case, it is hypothesized that the rate of carbon deposition observed is the catalytic

[5] For example,

$$3Fe + C \rightarrow Fe_3C$$

$\Delta V° \equiv \Sigma \nu_i V_i°$ (by definition); $\Delta V° = 23.41 - 5.33 - 3(7.09)$; $\Delta V° = -3.19$ cm³/gmol.

rate of pure Ni metal, whether in the reduced metal-phase field or in the carbide-phase field. It is interesting to recall that as the O/H ratio decreases the rate of weight gain increases. It was assumed that this is the result of one or two possible events: CH_4 as a preferential carbon source, or H_2 as a means to keep the active surface "clean." With regard to these two possibilities, Fig. 16 is illustrative. Figure 16 is a plot of weight gain versus time at 900 K, 1 bar, O/H = 0.25, and $\hat{a}_c = 10.8$ for Ni (open symbols) and Co (partially filled symbols). After approximately 125 min for Co and 170 min for Ni, the five-component gas mixture was switched to a binary gas mixture of 60% CH_4 and 40% H_2. As shown, Ni has a steady rate of weight gain regardless of whether CO is present or not. Cobalt, on the other hand, shows an exponential increase in weight gain with time under the five-component gas mixture, but the rate drops by an order of magnitude when switched to CH_4/H_2 mixture. One concludes that over Ni, not too surprisingly, CH_4 is the main source of carbon and the carbon deposited results primarily in filament growth. Over Co, and to a lesser extent over Fe, CH_4 only produces a small fraction of the carbon deposited. The vast majority of the measured weight gain over Co and Fe can be attributed to CO. The micrographs presented in this work suggest that, on Co foils and to a smaller extent on Fe foils, the majority of this carbon is amorphous in nature.

CONCLUSIONS

In the form of high-purity foils exposed to gases favoring carbide formation, Fe has a higher carbon deposition activity than Co, and Co is better than Ni. In the reduced metal region all three metals have similar low-carbon deposition activities (although they do appear to show similar ordering). The primary reason for higher carbon deposition activity for Fe and Co foils is hypothesized to be due to carbide formation and the associated area increase that results through surface break up. The ordering of carbon deposition activity is proportional to the carbide decomposition temperature. The higher carbon deposition rate is associated with the carbides with the higher decomposition temperature. Amorphous, flake, and filamentous carbons are observed to form on Fe and Co foils, and the deposition is relatively uniform over the surface.

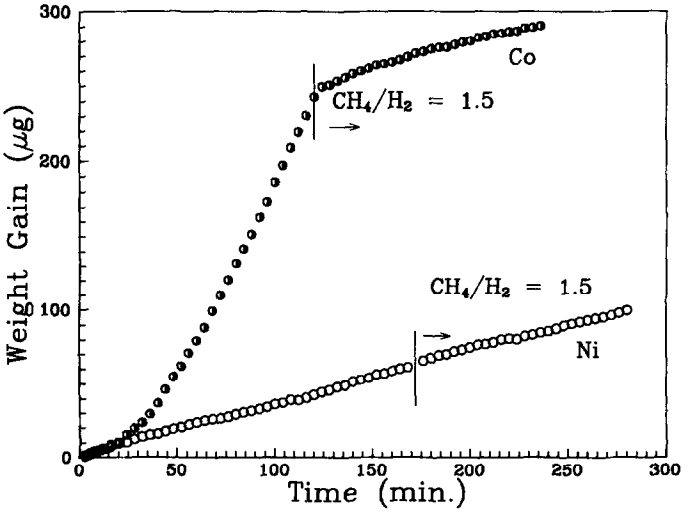

FIG. 16. Weight gain vs time over Co and Ni foils reacted at $\hat{a}_c = 10.8$ in two different gas environments.

However, on Ni foils deposition is area-dependent and is mostly filamentous in nature. The primary source of carbon for filament growth over Ni appears to be CH_4.

ACKNOWLEDGMENTS

The financial support and encouragement of NSF is gratefully acknowledged. Also, the assistance of Professor R. D. Sisson, Jr., Professor R. R. Biederman, and Mr. George Schmidt on the interpretation of the XRD data and electron micrographs was invaluable.

REFERENCES

1. MacIver, D. S., and Emmett, P. H., *J. Phys. Chem.* **59,** 1109 (1955).
2. Boehm, H. P., *Carbon* **11,** 583 (1973).
3. Oberlin, A., and Endo, M., and Kayama, T., *J. Cryst. Growth* **32,** 335 (1976).
4. Endo, M., Katoh, A., Sugiura, T., and Shiraishi, M., *Ext. Abstr. Program 18th Bienn. Conf. Carbon,* 151, 1987.
5. Walker, P. L., Jr., Rakszawski, J. F., and Imperial, G. R., *J. Phys. Chem.* **73,** 133 (1959); *J. Phys. Chem.* **73,** 140 (1959).
6. Ruston, W. R., Warzee, M., Hennaut, J., and Waty, J., *Carbon* **7,** 47 (1969).
7. Baker, R. T. K., Harris, P. S., Thomas, R. B., and Waite, R. J., *J. Catal.* **30,** 86 (1973).
8. Rostrup-Nielsen, J., and Trimm, D. L., *J. Catal.* **48,** 155 (1977).
9. Tibbetts, G. G., Devour, M. G., and Rodda, E. J., *Carbon* **25,** 367 (1987).
10. Kock, A. J. H. M., DeBokx, P. K., Boellaard, E., Klop, W., and Geus, J. W., *J. Catal.* **96,** 468 (1985).
11. Sacco, A., Jr., Thacker, P., Chang, T. N., and Chiang, A. T. S., *J. Catal.* **85,** 24 (1984).
12. Alstrup, I., *J. Catal.* **109,** 241 (1988).
13. Sacco, A., Jr., and Caulmare, J. C., *in* "Advances in Chemistry" (L. F. Albright and R. T. K. Baker, Eds.), Vol. 202, pp. 177–191. ASC Washington, DC, 1982.
14. Thacker, P., and Sacco, A., Jr., *in* "Proceedings, 8th International Conference on Catalysis, Berlin, 1984," Vol. 11, p. 647. Dechema, Frankfurt-am-Main, 1984.
15. Manning, M. P., Gamirian, J. E., and Reid, R. C., *Ind. Eng. Chem. Process Des. Dev.* **21,** 404 (1982).
16. Stull, D. R., "JANAF Thermochemical Tables," US Department of Commerce, Springfield, VA, 1965.
17. McCarty, J. G., and Wise, H. J., *J. Catal.* **57,** 406 (1979).
18. Rostrup-Nielsen, J. R., *J. Catal.* **27,** 343 (1972).
19. Debokx, P. K., Kock, A. J. H. M., Boellaard, E., Klop, W., and Geus, J. W., *J. Catal.* **96,** 454 (1985).
20. Nagakura, S., *J. Phys. Soc. Japan* **16,** 1213 (1961).
21. Hofer, L. J. E., Cohn, E. M., and Peebles, W. C., *J. Phys. Colloid Chem.* **53,** 661 (1949).
22. Audier, M., Coulon, M., and Bonnetain, L., *Carbon* **21,** 93 (1983).
23. Audier, M., Coulon, M., and Bonnetain, L., *Carbon* **21,** 99 (1983).
24. Audier, M., Coulon, M., and Bonnetain, L., *Carbon* **21,** 105 (1983).
25. Jackson, P. R. S., Trimm, D. L., and Young, D. J., *J. Mater. Sci.* **21,** 3125 (1986).
26. Hofer, L. J. E., Cohn, E. M., and Peebles, W. C., *J. Phys. Chem.* **54,** 1161 (1950).
27. Baird, T., Fryer, J. R., and Grant, B., *Carbon* **12,** 591 (1974).
28. Leidheiser, H., Jr., and Gwathmey, A. T., *J. Amer. Chem. Soc.* **70,** 1206 (1948).
29. Kehrer, V. J., and Leidheiser, H., Jr., *J. Phys. Chem.* **58,** 550 (1954).
30. Renshaw, G. D., Roscoe, C., and Walker, P. L., Jr., *J. Catal.* **22,** 394 (1971).
31. Audier, M., Oberlin, A., and Coulon, M., *J. Cryst. Growth* **55,** 549 (1981).
32. Bianchini, E. C., and Lund, C. R. F., *J. Catal.* **117,** 455 (1989).